Application of handheld/portable spectroscopic tools to the identification, inner stratigraphy and mapping of archaeological metal artefacts

Journal of Physics: Photonics

OPEN ACCESS

RECEIVED
17 December 2023

REVISED
17 April 2024

ACCEPTED FOR PUBLICATION
1 May 2024

PUBLISHED
13 May 2024

PAPER

Application of handheld/portable spectroscopic tools to the identification, inner stratigraphy and mapping of archaeological metal artefacts

Sara Mattiello[1,2], Olga De Pascale[1], Vincenzo Palleschi[3], Girolamo Fiorentino[4] and Giorgio S Senesi[1,*]

[1] CNR—Istituto per la Scienza e Tecnologia dei Plasmi (ISTP)—Sede di Bari, Via Amendola 122/D, 70126 Bari, Italy
[2] Physics Section, School of Science and Technology, Università di Camerino, via Madonna delle Carceri, 62032 Camerino, Italy
[3] CNR—Istituto di Chimica dei Composti Organo-Metallici (ICCOM), U.O.S. di Pisa, Pisa, 56124, Italy
[4] Laboratory of Archeobotany and Paleoecology, Department of Cultural Heritage, University of Salento, via Birago 64, 73100 Lecce, Italy
[*] Author to whom any correspondence should be addressed.

E-mail: giorgio.senesi@cnr.it

Keywords: laser-induced breakdown spectroscopy (LIBS), energy dispersive x-ray fluorescence (ED-XRF), handheld/portable instrumentation, copper and iron alloy archaeological artefacts, elemental detection and quantification, depth profiling, mapping

Supplementary material for this article is available online

Abstract

Field handheld/portable instrumentations, such as *in-situ* geochemical analyzers, have the potential to assist efficiently targeted geochemical archaeometry campaigns in detecting and quantifying specific elements. Non-destructive portable energy dispersive x-ray fluorescence and micro-destructive handheld laser-induced breakdown spectroscopy (LIBS) instrumentation were utilized to investigate the elemental composition, internal stratigraphy by depth profiling and microscale compositional mapping of five copper and two iron alloy artefacts collected from various ancient graves in the Minervino Murge area, Apulia, Italy. The primary elements identified by both techniques included Cu, Sn and Pb in copper alloys, and Fe with minor amounts of Cu and Pb in iron alloys. Furthermore, the elements Al, Ca, Si, Mg, Na and K, mostly originated from soil contamination, and the trace elements Sb, Ni and Zn were detected. The satisfactory performance of both techniques was assessed by their capacity to provide reproducible elemental composition data. Finally, the depth profile and mapping achieved by LIBS contributed to understanding the metal processing and history of the objects studied, so confirming both techniques to be robust analytical tools in outdoor archaeology and archaeometry campaigns.

1. Introduction

Throughout the last 7000–8000 years, metals have played a key role in shaping the course of human history by exerting a significant influence on the technological, socio-economic and political development. Various metal alloys with distinct properties, compositions and applications have been constructed and used during human history, which determined the beginning of the various Metal Ages and the consequent technological evolution [1]. For this reason, metal objects collected in archaeological excavations are highly appreciated for their intrinsic historical value.

The study of archaeological artefacts by archaeometric methods is instrumental to gain information on their fabrication, use and burial [2]. In particular, the evolution of metal alloys types over time has contributed to assign the production period and the classification of metal objects by measuring their quantitative elemental composition. For example, during the early bronze age, bronze-based alloys had a relatively high As content. Subsequently, during the middle bronze age, Sn replaced As with the final use of Sn-Pb alloys in the late bronze age, and then Fe in the iron age [3].

Obviously, the procedures and techniques to be used in the analysis of archaeological artefacts need to be less destructive as possible to preserve their integrity, i.e., avoid any removal of material. Typically, non-destructive analytical techniques, such as x-ray fluorescence (XRF), x-ray diffractometry and Raman spectroscopy, are the preferred ones [2]. However, the minimally destructive laser-induced breakdown spectroscopy (LIBS) features several relevant advantages, including rapidity, no sample preparation, capacity of performing multielement analysis, detection of any element of the periodic table including light elements, achievement of micro destructive compositional in-depth profile analysis, and rastering the laser beam across the sample surface in small steps to obtain a microscale compositional mapping [4, 5]. In particular, since the laser creates a tiny crater on the sample's surface, the continued firing of laser is able to penetrate below the corrosion layer, so allowing the in-depth analysis of the entire sample. This is an advantage with respect to the completely non-destructive measurements achieved by XRF, which, however, has limitations for measuring elements with low atomic number and can provide integrated information on the composition of the samples only for the entire volume. This does not allow to separate the information on the inner composition of the object from that of the surface, which in most cases is not representative of the whole object, due to effects of formation of patinas and corrosion, among others [6, 7]. Additionally, owing to variations in x-ray absorption by the elements, the effective volume of analysis is different for different elements, so that the XRF spectra frequently feature an intricate combination of fluorescence lines emitted by elements at depths extending several tens of microns beneath the surface [8].

Furthermore, recent studies have demonstrated that the mechanical cleaning typically needed before XRF analysis may produce intragranular corrosion on the surface, thus failing to provide the correct information on the original metal [9–11]. Additionally, the mechanical cleaning of historical artefacts is often prohibited, which favours the choice of LIBS analysis. Although the potential of handheld LIBS instrumentation has not yet been fully explored and its applications to archaeological metals analysis have been still sporadic [12], the application of LIBS in the sector of archaeological cultural heritage studies has been investigated and proven effective, for example in analysing glaze, the decorative layer composition of ceramics [13–15] and metallic objects [16–22].

Given the intrinsic fragility of some archaeological objects, their transport to the analytical laboratory should be avoided. Thus, movable instrumentations, such as portable energy dispersive (ED)-XRF and LIBS instruments, have emerged as very promising means for analysing archaeological artefacts both *in-situ* in field archaeological campaigns and directly in museums. A further advantage of both instruments is that they are equipped with internal protection systems that do not allow their operation if the sample is not in direct contact with the instrument, so limiting the operator's exposure to ionizing radiation for ED-XRF and avoiding the use of protective glasses for LIBS [5].

The objective of this research was to assess the feasibility of the combined use of handheld LIBS and portable ED-XRF instrumentations in: (a) identifying and quantifying *in-situ* the elemental composition of copper and iron alloy artefacts collected from various ancient graves in the Minervino Murge area, Apulia, Italy; (b) evaluating the presence of a patina and different underlying layers by in-depth profiling so achieving their inner stratigraphy; (c) mapping their surface; and (d) establishing correlations between the compositional data and the technological features, possibly confirming the archaeological dating of the objects.

2. Materials and methods

2.1. Samples

The samples investigated in this work were seven artefacts, five made of copper alloy, i.e. a belt (A), a basin (B), a fibula (C), a helm (D) and a pendant (E), and two made of iron alloy, i.e. a dagger/knife (F) and a spatula (G) (figure 1). All objects, dated by archaeological criteria, such as shape, feature and use, as belonging to the VI century B.C., were collected in an iron age necropolis located in the area of Minervino Murge, Apulia, Italy, and immediately transferred to the Soprintendenza Archeologia, Belle Arti e Paesaggio per le Province di Barletta—Andria—Trani e Foggia for conservation and restoration. The artefacts were in a relatively good preservation state and showed a thin, relatively uniform patina on the surface, but also more degraded areas. The main interest of archaeologists was to know the elemental composition of the artefacts, in order to improve the knowledge of their technical production and confirm the archaeological period.

The belt is composed of three laminas connected by nails and had the function of fastening cloths. The basin fragment features an edge worked by chisel and was used as container of water or food. The fibula was a sort of brooch and had mainly the function of stopping or closing cloths, such as cloaks and tunics. The helm fragment does not allow to identify the type of helm to which it belonged. The pendant, which had a decorative function, consists of a thin flat bronze sheet of vaguely trapezoidal shape and features a small hole positioned approximately halfway along the upper side. The dagger/knife is heavily oxidized and shows

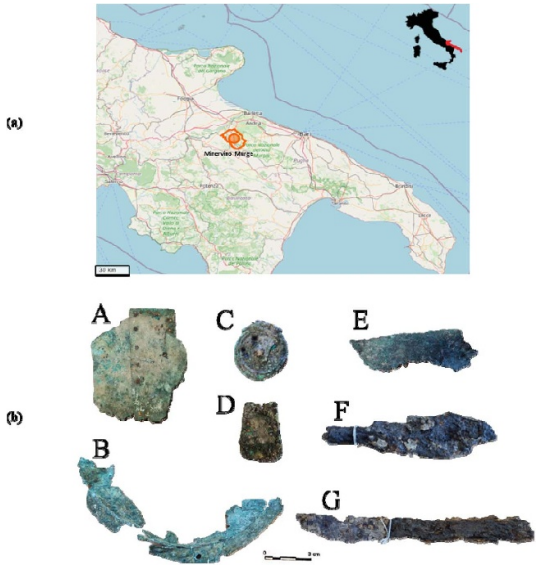

Figure 1. Location of the Minervino Murge site in the region of Apulia, Italy (a) and photos of the archaeological objects studied (b). Copper alloys: belt (A), basin (B), fibula (C), helm (D), pendant (E); iron alloys: dagger/knife (F) and spatula (G).

evident signs of solidified glue due to previous restorations. The spatula might have been used in religious contexts during ceremonies and rituals. All the artefacts appear to belong to a funeral kit.

No sample removal and neither mechanical nor solvent cleaning were performed on the objects prior to analysis. The different shapes and sizes of the objects were not a limitation for analysis, as they were placed in front of and in contact with the head of the instrument.

2.2. ED-XRF and LIBS analysis

The portable ED-XRF instrument used was a SciAps X-200 (Woburn, MA, USA) powered by an on-board rechargeable Li-ion battery and having dimensions of 18 × 27 × 11 cm and weight of 1.5 kg. The spectra were acquired in Alloy mode, which allowed the quantitative determination of elemental composition using specific reference libraries. Two measurements were used for the detection of the elements, using x-ray tube voltage of 40 kV for heavy elements and 10 kV for light ones, with an exposure time of 30 sec. The analysed area is around 8-mm of diameter.

The handheld LIBS instrument used was a SciAps Z-903 (Woburn, MA, USA) powered by an on board Li-ion battery and having dimensions of 27 × 22 × 7 cm and weight of 1.97 kg. The device uses a Class 3B 1064 nm Nd:YAG diode-pumped solid-state pulsed laser, which fires at a rate of 1–50 Hz and generates a 100 μm focused beam that provides a 5–6 mJ pulse to the sample in a 1-ns pulse. The instrument covers a spectral range from 190 to 950 nm, over which each element features at least one emission line. The spectral data were collected at a 650-nsec delay time over a 3-msec integration time. The elemental depth profiles of samples were collected at a laser firing rate of 10 Hz employing 128 successive laser shots in a single location, after one cleaning shot.

Ten measurements were acquired by both XRF and LIBS on the same points of each sample to obtain its representative average composition and mapping the variability of the bulk composition of the object. The LIBS depth profiles were measured on five points of each object. The Geochem Pro mode of the Z-903 LIBS instrument was used to identify spectral peaks and then generate the corresponding concentration microscale maps based on the relative elemental emission intensities recorded. The two-dimensional (2D) maps, commonly called 'heat maps', were obtained on six relatively flat surface areas of object A using single laser shots spaced 25 μm each other at 256 locations/points over a 16 × 16 grid covering an area of 2 mm^2.

3. Results and discussion

3.1. ED-XRF

The main elements detected with different relative intensity by ED-XRF were Cu, Sn, Pb and Fe in copper alloys and mostly Fe in iron alloys (figures 2(a) and (b)). These elements were identified based on their characteristic emission lines, i.e. Cu ($K\alpha$ at 8.04 keV and $K\beta$ at 8.9 keV), Sn ($K\alpha$ at 25.27 keV), Pb ($L\alpha$ at 10.55 keV and $L\beta$ at 12.6 keV) and Fe ($K\alpha$ 6.4 keV and $K\beta$ at 7.05 keV) [23].

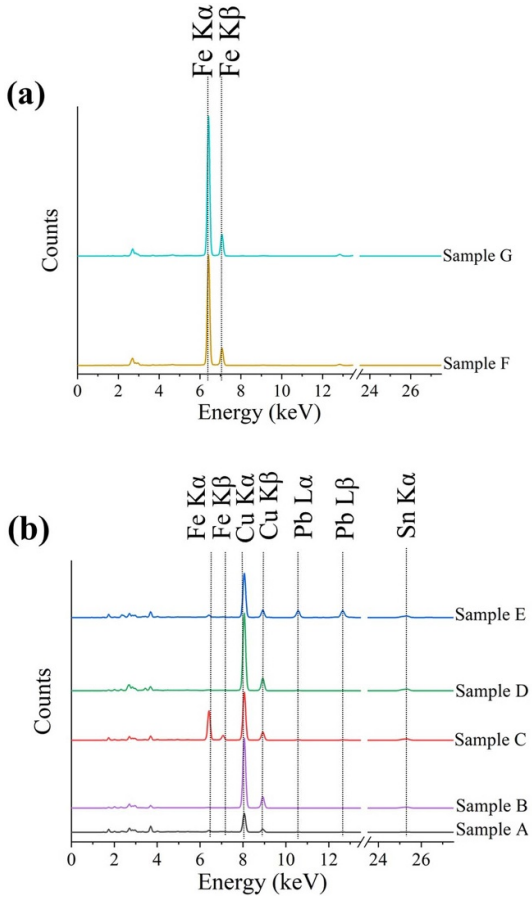

Figure 2. Representative ED-XRF spectra of iron alloy objects (a) and copper alloy objects (b), where the energy in keV is reported in the *x* axis and the counts in the *y* axis. The dashed lines indicate the main fluorescence lines of Fe, Pb, Sn and Cu.

Table 1. Average concentration (wt %) and standard deviation (SD) of the main elements identified by the portable ED-XRF instrument in the studied artefacts.

Samples	Elements							
	Fe	SD	Cu	SD	Sn	SD	Pb	SD
A (belt)	0.895	0.13	73.35	4.6	5.39	3.22	2.998	2.55
B (basin)	0.387	0.05	80.6	1.98	6.26	1.32	0.277	0.07
C (fibula)	7.288	7.07	66.74	3.43	5.82	2.92	1.478	0.51
D (helm)	0.224	0.2	82.28	4.26	6.52	2.1	0.288	0.13
E (pendant)	1.828	0.57	46.95	6.29	6.16	3.16	24.14	9.8
F (dagger)	96.94	2.03	0.225	0.12	ND	—	0.05	0.02
G (spatula)	98.28	0.78	0.22	0.13	ND	—	0.048	0.03

ND: not detected.

The quantitative elemental analysis of the alloys was referred to the reference standards included in the instrument database. The average concentration and the standard deviation (SD) of the main elements in each object, measured following the 3σ rule with 99.7% level of confidence, as reported by the instrument, are listed in table 1, whereas the complete list of element concentrations is reported in table S1 in supplementary information (SI). These values, however, should be taken with great caution because ED-XRF is a volume technique and, as such, is sensitive to the possible compositional variations below the surface of the sample, due to corrosion or depending on the technique used for their realization. In that respect, LIBS analysis would provide unique information about the in-depth variations of sample composition, so allowing to assess the reliability of ED-XRF quantitative analysis.

3.2. LIBS

The broadband LIBS spectra of iron alloy and copper alloy objects are shown, respectively, in figures S1(a) and S1(b) in the SI, whereas the emission lines of interest and their attribution based on the NIST database [24] are summarized in table 2. The main elements detected in copper alloys were Sn, Cu and Pb (figure 3)

Table 2. LIBS atomic (I) and ionic (II) emission lines used to identify elements in the studied artefacts.

Element	Wavelength (nm)
Na	588.9 (I); 589.6 (I)
Mg	279.6 (II); 280.3 (II); 285.2 (I); 448.1 (II)
Al	309.3 (I)
Si	251.6 (I); 288.2 (I)
K	766.5 (I); 769.9 (I)
Ca	393.4 (II); 396.8 (II); 422.7 (I); 430.3 (I); 445.5 (I)
Fe	259.8 (II); 259.9 (II); 274.0 (II); 275.6 (II); 364.8 (I); 372.0 (I)
Ni	338.1 (I)
Cu	224.3 (II); 224.7 (II); 324.8 (I); 327.4 (I); 465.1 (I); 510.6 (I); 515.3 (I); 521.8 (I)
Zn	202.5 (II)
Sn	190.0 (II); 283.9 (I)
Sb	217.9 (I); 247.8 (I); 252.9 (I)
Pb	261.4 (I); 283.3 (I); 364.0 (I); 368.3 (I); 405.7 (I)

and mainly Fe and minor contents of Cu and Pb in iron alloys. Other elements detected in the samples oxidation layer were Al, Ca, Si, K, Na and Mg, which originated very probably from soil contamination (figure 3(d)). Furthermore, the elements Sb, Ni and Zn were identified in trace amounts. Pyrometallurgically produced Cu contains several accidental impurities such as Sb, As, Ni, Ag and many others that may replace Cu in several minerals [1]. The amount of impurities depends on several factors, such as ore dressing, roasting, smelting and refining technologies. Anyhow, all impurities affect significantly the microstructure and properties of a Cu alloy, but the extent of their effects depend on their typology, content and solubility [1].

Copper-alloy objects showed similar emission lines with Cu being the major component, and the main difference being the variable intensity of the Sn emission. In this respect, for example, sample A showed a large variability of the intensity of the emission lines of Sn and Pb between the various points measured on the lamina. As expected, the iron-alloy objects F and G showed a predominance of Fe emission lines and minor amounts of Cu and Pb (less than 1 wt%, according to XRF analysis) (figure S1(a)). The different lines intensities of the main elements (Cu, Sn and Pb) among copper alloy samples (figure 3) may be ascribed to the different heat treatment during their manufacturing and/or to the different environmental degradation that the object has suffered over time. In particular, various environmental factors, such as variations in temperature and humidity, would have generated alterations of the structure and chemical composition of ancient metal alloys, with possible impacts on the reliability of quantitative elemental analysis [20]. The absence of As suggested that the objects were dated correctly, as the presence of As, usually between 2 and 8 wt% in copper alloys, is typical of the early Bronze Age. In particular, the presence of As allowed the alloy to be hammered without breakage and made it particularly suitable for casting. Its absence also suggested that the bronzes under analysis were not made by recycling of older objects [22].

The results of artefacts analysis by the two techniques contributed to focus on sample A, the belt, as the most interesting object studied. By visual inspection, the belt appeared composed of three different pieces of metal connected each other by small nails (figures S2(a) and (b) in SI). Furthermore, the laminas showed an inhomogeneous composition in the different points analysed. Thus, microscale LIBS mapping was performed on sample A with the purpose of identifying the most appropriate surface points where to perform a LIBS depth profile analysis.

The generation process of 2D elemental concentration maps or 'heat maps' is based on the spectral peak intensities derived from individual laser shots spaced across the sample. i.e. it involves a detailed and localized exploration of the sample elemental composition, which allows an efficient evaluation of the distribution and concentration of each element within the microscale domain. Apparently, the elemental components, i.e, Cu, Sn, Pb, Ca, Fe, Cr, P, Si, Na, K and Sb, of the three laminas on sample A surface featured a different distribution (figure S2). In particular, Sn is not detected in lamina 2, whereas this element is abundant in the back of lamina 1 (figure S2(d)). Furthermore, the presence of Cu in lamina 2 was lower than in the other two laminas probably due the thickness of the oxidation patina and the presence of soil contaminants. No differences were apparent between the composition maps of the front and back sides of the object, with the exception of Sn in lamina 1 and Ca in lamina 2, which are more abundant on the back side. Although the objects were cleaned after their collection, they show concretions on the surface due to soil deposition and oxidation patinas. The complex layered structure of patinas can be related to the use of the object (primary patina) and the chemical reactions occurred during its permanence in soil (secondary and tertiary patina) [2]. The absence of Cl in all laminas suggested good preservation conditions, whereas its

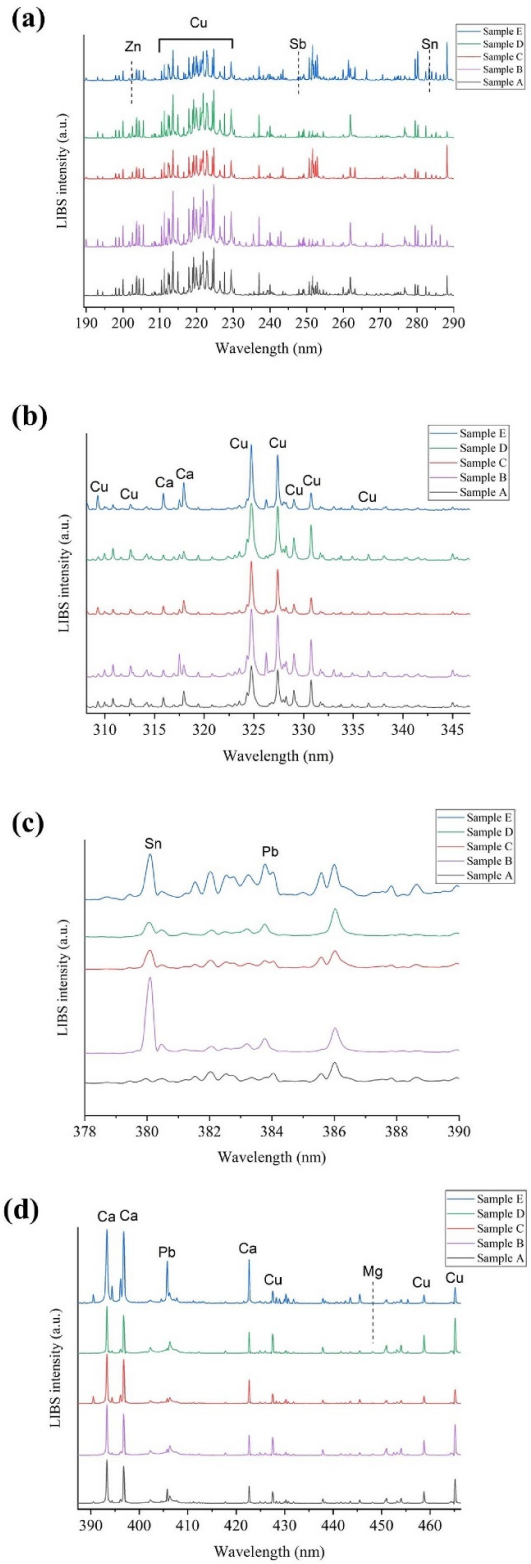

Figure 3. Detailed representative LIBS spectral ranges of copper alloy objects. (a) Spectral range from 190 to 290 nm with Zn, Cu, Sb and Sn emission lines identified; (b) spectral range from 310 to 345 nm with Ca and Cu emission lines identified; (c) spectral range from 378 to 390 nm with Sn and Pb emission lines identified, (d) spectral range from 385 to 465 nm with Ca, Pb, Cu and Mg emission lines identified.

presence would suggest the existence of the so-called 'vile' patina characterized by chloride salts that contribute to the pulverization of metals [25]. Thus, the core of the alloy under the 'noble' patina appeared to have been protected from oxidation processes.

The analysis of depth profiles can provide the composition of the alloy core below the corrosion layer, so achieving unique information on the processing technique used to construct the object. The depth profiles

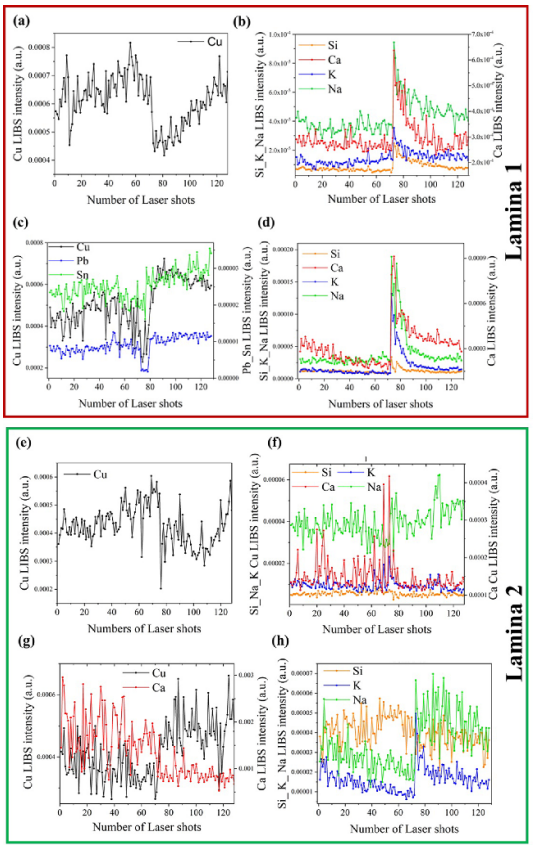

Figure 4. Depth profiles of sample A: front side (a), (b) and back side (c), (d) of lamina 1; front side (e), (f) and back side (g), (h) of lamina 2.

were achieved for the front side (a), (b) and back side (c), (d) of lamina 1 and lamina 2 (respectively, (e), (f) and (g), (h)) at depths of 10 μm for each laser shot by measuring the peak areas of the reference emission lines selected, i.e. Cu I (465.11), Sn I (283.99), Pb I (368.34), Si I (288.2), Ca I (422.7), K I (766.5) and Na I (588.9), as a function of the number of laser shots (figure 4). The LIBS signals of Pb and Sn were detected only for the back side of lamina 1 (figure 4(c)). For both front and back side of lamina 1, at the depth reached after 60–80 laser shots, a sharp change in the intensity of LIBS signals was measured (figures 4(a)–(d)). In particular, the Cu, Pb and Sn signals decreased and then increased again (figures 4(a) and (c)), whereas those of Si, K, Na and Ca increased and then decreased (figures 4(b) and (d)). These results would suggest that lamina 1 features two distinct oxidation layers. Differently, for lamina 2 after about 60–80 shots, the intensity of Cu signals decreased abruptly and then remained almost constant in the front side (figure 4(e)), whereas the opposite occurred in the back side (figure 4(g)). Only the intensity of Ca in the front side and those of K and Na in the back side of lamina 2 showed an abrupt increase after 60–80 laser shots and then returned to the previous values, whereas the intensity of the other elements due to soil contamination appeared not to change significantly as a function of increasing depth (figures 4(f) and (h)).

Based on the elemental maps and depth profiles data, it appears that the thickness of the oxidation layer(s) (600–800 μm) is much larger than the typical penetration depth of ED-XRF, which is about 100–200 μm, depending on the elements. The quantitative data reported in table 1 must be thus reconsidered, taking into account the changes in the elemental LIBS signal intensity (roughly proportional to the element concentration) under the corrosion layer. For example, the depth profiles in figure 4(c) show that the Sn and Pb signal intensities remain roughly constant down to 500 μm below the surface, while the Cu line intensity at the surface is about 20% lower than that at 500 μm depth.

Typically, a bronze alloy containing from 8 to 12 wt% Sn has a combination of hardness and plasticity that makes it easily workable at low temperatures [22]. Thus, the estimation of a Sn concentration lower than 10 wt% achieved by ED-XRF allowed to conclude that the copper alloy artefacts examined were manufactured by the cold hammer technique. If the percentage of Sn exceeds 12 wt%, the increased hardness and brittleness of the alloy make handling at low temperatures difficult and can lead to breakage of the material [26], i.e. the alloy becomes harder and requires repeated annealing cycles to be handled. However, a bronze with a Sn content above 12 wt% is more suitable for hot working.

A content of Pb lower than 3 wt% measured in all copper alloys, except sample E, might be ascribed to impurities present in the raw copper material used, e.g. smelting galena or other copper minerals containing Pb [1]. Differently, the high Pb content in sample E was likely attributable to surface enrichment phenomena due to the hammering process [27]. In particular, a content of Pb below 2 wt% supported the hypothesis of cold hammering. Differently, an amount of Pb higher than 2 wt% would indicate its intentional addition to bronze, in order to lower the melting point of the alloy and improve its casting properties [28].

Furthermore, the different concentration of the main elements in the two laminas of object A suggested that they were produced at different times and connected to each other after the object was repaired. In particular, the Sn signal was not detected in all analytical points, especially where its amount was lower than 6 wt% (as calculated by ED-XRF quantitative analysis).

4. Conclusions

The two instruments used in this study, i.e. handheld LIBS and portable ED-XRF, have been shown to be versatile, efficient and complementary for the *in-situ* analysis of archeological metal artefacts directly in the museum or in the field under ambient environmental conditions. In particular, the primary benefits of LIBS include its relatively quick and easy analytical process (few sec), the need of little or no sample preparation, the ability to analyze multiple elements at once and in specific sample regions and to achieve compositional depth profiling and surface microscale chemical mapping on a spatial scale of about 10 μm. However, in order to achieve quantitative results LIBS requires calibration using matrix-matched standards. On the other hand, the primary advantages of ED-XRF include its inherent calibration from the factory, which works well with a variety of sample types, and its ease of use for quantitative analysis in the field. The ED-XRF, however, needs a 1-to 2 min analytical time, depending on the required precision and detection limits, and is unable to measure elements with atomic numbers lower than Si.

Moreover, as the two techniques perform on very different volumes, the quantitative analysis provided by the ED-XRF technique cannot be trusted in the presence of surface corrosion layers or, in general, in-depth inhomogeneities, whereas LIBS is a tool more suitable for the analysis of patinas and corrosion layers. In particular, the area that LIBS can analyze has a diameter of around 100 μm with a depth of around 10 μm per laser pulse. Differently, ED-XRF can typically analyze a surface area of around 8 mm diameter (although it can be reduced to about 3 mm), with a depth of analysis strictly related to the x-ray attenuation that depends on energy, material and angle, but in any case of the order of several tens of microns.

In this work, the quantitative elemental composition of five copper alloy and two iron alloy archaelogical artefacts has been measured, i.e. Cu, Sn and Pb in copper alloys, and Fe with minor amounts of Cu and Pb and some trace elements Sb, Ni and Zn in iron artefacts. In particular, ED-XRF provided the quantitative estimation of the elements concentrations in the first 100–200 μm under the surface, and LIBS complemented this evaluation by measuring the in-depth variation of the sample composition. The LIBS depth profiling and mapping of the artefacts also allowed to distinguish among the different corrosion layer and hypothesize the processing technique used to construct and/or repair them. The analytical results obtained have shown that the copper alloy objects were made of bronze whose content of Sn was typical of the Iron Age, which was confirmed by the absence of As that also allowed to exclude recycling of more ancient objects. Finally, the depth profile results suggested that cold hammering was the copper alloy processing used.

In conclusion, the results of this work suggest that the instruments employed appear appropriate for the quantitative elemental analysis of archaeological metal artefacts, which is also confirmed by the good agreement with literature data regarding ancient bronze. In particular, handheld/portable instruments have shown stability in measurements over time, satisfactory reproducibility and a good balance between resolution and size, rendering them an excellent option for direct *in-situ* analysis of archaeological metal artefacts in museums, outdoor campaigns and in hardly accessible places.

Data availability statement

The data cannot be made publicly available upon publication because they are not available in a format that is sufficiently accessible or reusable by other researchers. The data that support the findings of this study are available upon reasonable request from the authors.

Acknowledgments

The authors acknowledge the financial support received under the project MIUR D D n. 2284, 29 September 2021, PRIN 'UNDERLANDSCAPE: a multi-analytic approach to the study, conservation and valorization of the underground historical environment and the surrounding landscape', Smart Ndt and SciAps for

providing us the use of X-200 portable ED-XRF instrument, and the Soprintendenza Archeologia, Belle Arti e Paesaggio per le Province di Barletta—Andria—Trani e Foggia for authorizing the analyses (M Corrente and I M Muntoni).

ORCID iDs

Sara Mattiello https://orcid.org/0009-0000-9601-4703
Olga De Pascale https://orcid.org/0000-0002-7220-1069
Vincenzo Palleschi https://orcid.org/0000-0002-6377-7656
Girolamo Fiorentino https://orcid.org/0000-0001-8480-891X
Giorgio S Senesi https://orcid.org/0000-0002-3947-6853

References

[1] Scott D A and Schwab R 2019 *Metallography in Archaeology and Art* (Springer)
[2] Di Turo F 2019 Limits and perspectives of archaeometric analysis of archaeological metals: a focus on the electrochemistry for studying ancient bronze coins *J. Cult. Herit.* **43** 271–81
[3] Radivojević M *et al* 2019 The Provenance, use, and circulation of metals in the European Bronze Age: the state of debate *J. Archaeol. Res.* **27** 131–85
[4] Detalle V and Bai X 2022 The assets of laser-induced breakdown spectroscopy (LIBS) for the future of heritage science *Spectrochim. Acta* B **191** 106407
[5] Senesi G S, Harmon R S and Hark R R 2021 Field-portable and handheld laser-induced breakdown spectroscopy: historical review, current status and future prospects *Spectrochim. Acta* B **175** 106013
[6] Frahm E and Doonan R C P 2012 The technological versus methodological revolution of portable XRF in archaeology *J. Archaeol. Sci.* **40** 1425–34
[7] Pérez-Serradilla J A, Jurado-López A and Luque de Castro M D 2007 Complementarity of XRFS and LIBS for corrosion studies *Talanta* **71** 97–102
[8] Botto A, Campanella B, Legnaioli S, Lezzerini M, Lorenzetti G, Pagnotta S, Poggialini F and Palleschi V 2019 Applications of laser-induced breakdown spectroscopy in cultural heritage and archaeology: a critical review *J. Anal. At. Spectrom.* **34** 81–103
[9] Orfanou V and Rehren T 2015 A (not so) dangerous method: pXRF vs. EPMA-WDS analyses of copper-based artefacts *Archaeol. Anthropol. Sci.* **7** 387–97
[10] Nørgaard H W 2017 Portable XRF on prehistoric bronze artefacts: limitations and use for the detection of bronze age metal workshops *Open Archaeol.* **3** 101–22
[11] Gójska A, Mišta-Jakubowska E, Banaś D, Kubala-Kukuś A and Stabrawa I 2019 Archaeological applications of spectroscopic measurements. Compatibility of analytical methods in comparative measurements of historical Polish coins *Measurement* **135** 869–74
[12] Wallace S, Smith N and Nerantzis N 2021 Handheld methods in archaeological research on large copper alloy assemblages: HH-XRF against HH-LIBS *Archaeometry* **63** 343–71
[13] Colao F, Fantoni R, Lazic V and Spizzichino V 2002 Laser-induced breakdown spectroscopy for semi-quantitative and quantitative analyses of artworks—Application on multi-layered ceramics and copper based alloys *Spectrochim. Acta* B **57** 1219–34
[14] Melessanaki K, Ferrence S C, Betancourt P P and Anglos D 2003 Application of LIBS in the analysis of archaeological objects *19th Congress Int. Commission for Optics: Optics for the Quality of Life* (SPIE) p 79
[15] Lazic V, Vadrucci M, Fantoni R, Chiari M, Mazzinghi A and Gorghinian A 2018 Applications of laser-induced breakdown spectroscopy for cultural heritage: a comparison with x-ray fluorescence and particle induced x-ray emission techniques *Spectrochim. Acta* B **149** 1–14
[16] Fortes F J, Cortés M, Simón M D, Cabalín L M and Laserna J J 2005 Chronocultural sorting of archaeological bronze objects using laser-induced breakdown spectrometry *Anal. Chim. Acta* **554** 136–43
[17] Ferretti M, Cristoforetti G, Legnaioli S, Palleschi V, Salvetti A, Tognoni E, Console E and Palaia P 2007 In situ study of the Porticello Bronzes by portable x-ray fluorescence and laser-induced breakdown spectroscopy *Spectrochim. Acta* B **62** 1512–8
[18] Arafat A, Na'es M, Kantarelou V, Haddad N, Giakoumaki A, Argyropoulos V, Anglos D and Karydas A G 2013 Combined in situ micro-XRF, LIBS and SEM-EDS analysis of base metal and corrosion products for Islamic copper alloyed artefacts from Umm Qais museum, Jordan *J. Cult. Herit.* **14** 261–9
[19] Tankova V, Malcheva G, Blagoev K and Leshtakov L 2018 Investigation of archaeological metal artefacts by laser-induced breakdown spectroscopy (LIBS) *J. Phys.: Conf. Ser.* **992** 012003
[20] Fortes F J, Cabalín L M and Laserna J J 2020 Fast and in-situ identification of archaeometallurgical collections in the museum of Malaga using laser-induced breakdown spectroscopy and a new mathematical algorithm *Heritage* **3** 1330–43
[21] Ghervase L, Dinu M, Bors C, Anghelut L M, Radvan R and Cortea I M 2020 Investigation on metal adornments from ancient Eastern Europe *Front. Mater.* **7** 600913
[22] Penkova P, Malcheva G, Grozeva M, Hristova T, Ivanov G, Alexandrov S, Blagoev K, Tankova V and Mihailov V 2023 Laser-induced breakdown spectroscopy and x-ray fluorescence analysis of bronze objects from the late bronze age baley settlement, Bulgaria *Quantum Beam Sci.* **7** 22
[23] Thompson A C *et al* 2009 *X-ray Data Booklet* (Lawrence Berkeley National Laboratory, University of California)
[24] National Institute of Standard and Technology (available at: www.nist.gov/pml/atomic-spectra-database) (Accessed 14 November 2023)
[25] Scott D A 2000 A review of copper chlorides and related salts in bronze corrosion and as painting pigments *Stud. Conserv.* **45** 39–53
[26] Leoni M 1985 Elementi di metallurgia applicata al restauro delle opere d'arte *Corrosione e Conservazione dei Manufatti Metallici (Opus Libri)*
[27] Kareem K, Sultan S and He L 2015 Fabrication, microstructure and corrosive behavior of different metallographic tin-leaded bronze alloys part II: chemical corrosive behavior and patina of tin-leaded bronze alloys *Mater. Chem. Phys.* **169** 158–72
[28] Johannsen J W 2016 Heavy metal: lead in bronze age scandinavia *J. Swed. Antiq. Res.* **111** 153–61